Transition state dynamics of the OH + H_2O hydrogen exchange reaction studied by dissociative photodetachment of $H_3O_2^-$

Hans-Jürgen Deyerl, A. Khai Luong, Todd G. Clements and Robert E. Continetti

Department of Chemistry and Biochemistry, University of California, San Diego, 9500 Gilman Drive, La Jolla, CA, 92093-0314, USA

Received 6th December 1999
Published on the Web 9th May 2000

Dynamics in the transition state region of the bimolecular OH + $H_2O \rightarrow H_2O$ + OH hydrogen exchange reaction have been studied by photoelectron–photofragment coincidence spectroscopy of the $H_3O_2^-$ negative ion and its deuterated analog $D_3O_2^-$. The data reveal vibrationally resolved product translational energy distributions. The total translational energy distribution shows a vibrational progression indicating excitation of the antisymmetric stretch of the water product. Electronic structure calculations at the QCISD level of theory support this analysis. Examination of the translational energy release between the neutral products reveals a dependence on the product vibrational state. These data should provide a critical test of *ab initio* potential energy surfaces and dynamics calculations.

1. Introduction

Photoelectron–photofragment coincidence spectroscopy has proved to be a valuable method for studying dissociative photodetachment dynamics (DPD).[1] Dissociation occurs upon photodetachment when a stable anion has Franck–Condon overlap with repulsive regions of the corresponding neutral energy surface. For stable negative ions in a nuclear configuration similar to that of the transition state of a bimolecular reaction, photodetachment accesses the transition state region of the neutral potential energy surface. Our technique of studying the transition state dynamics builds on the innovative transition state spectroscopy experiments of Neumark *et al.*[2] and Wenthold and Lineberger[3] in which photoelectron spectroscopy is used to probe the transition state region of a chemical reaction. To fully characterize such DPD processes, a more complete measurement must be made. By combining the techniques of photofragment translational spectroscopy[4] and photoelectron spectroscopy,[5] the kinetic energies of the photoelectrons and photofragments can be measured in coincidence, providing a complete kinematic characterization of DPD.

In this paper we present the results of our recent studies of the dynamics of DPD in $H_3O_2^-$ giving insights into the dynamics of the fundamental hydrogen exchange reaction of the hydroxyl radical with water:

$$OH + H_2O \rightarrow H_2O + OH \quad (1)$$

These results shed light on the dynamics of dissociation on the neutral surface near the transition state of the bimolecular reaction. The experiments reveal a vibrationally resolved translational energy distribution after photodetachment of the corresponding negative ion ($H_3O_2^-$).

The hydroxyl radical is the predominant oxidant in the atmosphere, in combustion processes and in a wide range of other chemically active environments.[6] The thermoneutral identity reaction under study here is one of the simplest hydrogen abstraction reactions by the hydroxyl radical. This reaction is intrinsically interesting because the associated isotope exchange reactions may play a role in determining the isotopic composition of stratospheric water, providing a useful test of the validity of several atmospheric models.[7] On the fundamental level, this reaction is one of the simpler radical–molecule reactions and thus is of interest as a prototype.

Recent work on the kinetics of the neutral reaction has been published by Dubey *et al.*[7] Slow isotope exchange rates of hydroxyl radicals with water were observed and a correlation between theoretical (*ab initio*) and experimental reaction barriers was found to capture the overall reactivity trend. Photodetachment of the $H_3O_2^-$ anion was first studied by Golub and Steiner.[8] The total photodetachment cross section was measured as a function of photon energy up to 4 eV. The monotonic increase they observed in the photoelectron signal with increasing photon energy beyond 2.8 eV was interpreted as photodetachment from a chemically bound negative ion ($H_3O_2^-$) to a repulsive neutral complex, which separates to H_2O and OH. There have apparently been few studies of the chemical dynamics of this reaction outside of the transition-state-spectroscopy experiments of Arnold *et al.*[9] In the experiment of Arnold *et al.* the photoelectron spectra of $H_3O_2^-$ and the deuterated analog were recorded at 266 nm. The spectra show resolved vibrational progressions attributed to the antisymmetric hydrogen atom vibrational motion in the unstable neutral complexes formed by photodetachment.

Fig. 1 shows the schematic energy diagram for the $H_3O_2^-/OH + H_2O$ system. There have been several theoretical studies on the structure,[10–14] and the nature of the $H_3O_2^-$ potential.[9,15–17] The most detailed study[17] indicates a double well potential with a small barrier on the electronic surface. However, this barrier is below the lowest vibrational level, leading to an effective single well potential. The dissociation energy, $D_0(H_3O_2^- \rightarrow OH^- + H_2O) = 1.18$ eV has been measured

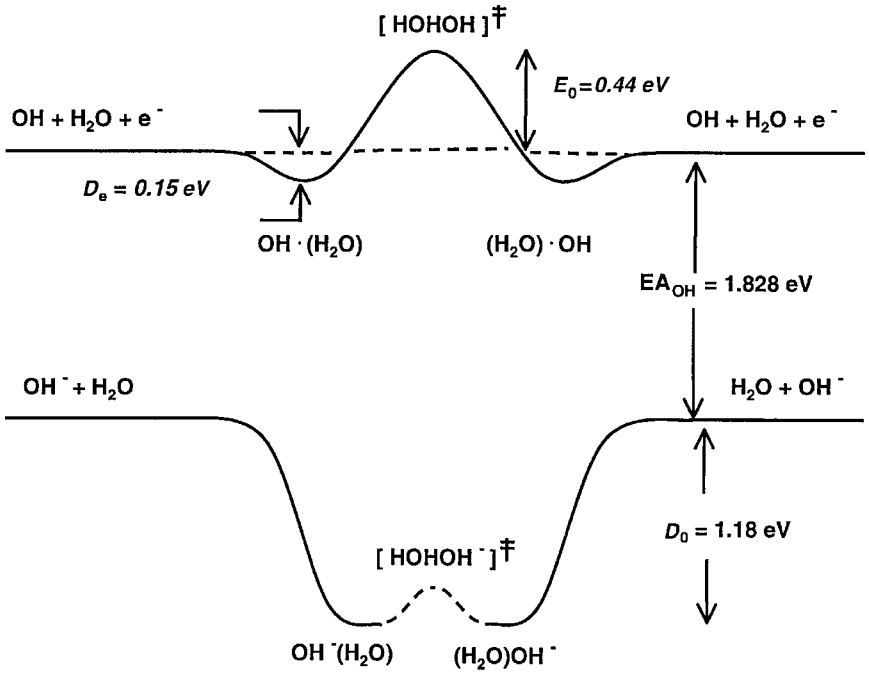

Fig. 1 Schematic energetics diagram for the $H_3O_2^-/OH + H_2O$ system. The potential energy is shown as a function of a generic reaction coordinate. The values in italics are theoretically determined values. For references see the text.

by high pressure mass spectrometry.[18] The electron affinity of the hydroxyl radical EA(OH) = 1.828 eV has been determined by threshold photodetachment of OH^-.[19] The neutral potential energy surface has been investigated by *ab initio* calculations of the stationary points. Schaefer and co-workers calculated several $(H_2O)^{\cdot}OH$ van der Waals minima,[20] with dissociation energies of 0.1 eV for the $^2A'$ state and 0.15 eV for the $^2A''$ state in the hydrogen bonded configurations, which are applicable to the photodetachment experiments. The global minimum ($^2A''$) was found to occur in a different nuclear configuration which is not conducive to hydrogen exchange and the dissociation energy was calculated to be 0.24 eV. The [HOHOH]‡ transition state (TS) has been theoretically studied in detail.[9,21–23] All results or assumptions have centered about a symmetric structure for the TS. However, calculations at the UMP2/6-311++G(2d,p) level of theory led to an asymmetric structure.[22,23] The symmetric structure of the transition state was confirmed by geometry optimization at the CCSD(T) and CASSCF(7,7) theory levels in the 6-311++G(2d,p) basis.[22] The best estimate for the barrier height was reported to be $E_0 = 0.44$ eV.[23]

2. Experimental

In these experiments, the DPD of $H_3O_2^-$ is studied by a coincidence measurement of the three photoproducts (electron + two neutral fragments). The experimental method has been previously described in detail,[1,24,25] and will be only briefly reviewed here. A fast beam of mass-selected negative ions ($H_3O_2^-$) is intersected with a pulsed laser beam and the kinematic properties of the photoelectron and neutral fragments are measured in coincidence. The apparatus consists of a mass-selected anion source, a photoelectron spectrometer and a photofragment translational spectrometer. High detection efficiencies and use of time and position-sensitive particle detectors for both the photoelectron and molecular fragments allow the correlated measurement of kinetic energy of all the products.

$H_3O_2^-$ is generated by crossing a continuous supersonic expansion of water (~4%) seeded in a gas-mixture of N_2O (~2%) and CH_4 (~94 %) with a 1 keV electron beam. $D_3O_2^-$ is produced by using D_2O instead of water, indicating fast isotopic scrambling in the source region. Anions are formed in this source through secondary electron attachment and three-body stabilization.[26] The nascent anions cool in the expansion and pass through a skimmer into a differentially pumped chamber where they are accelerated to beam energies of 2.5 and 4 keV. This was done to rule out formation of any long-lived (μs) neutral complexes. After acceleration, the continuous ion beam is referenced to ground potential and chopped using a pulsed potential switch. Anions are separated according to mass by time of flight (TOF). Fast neutral particles are removed by guiding the ion beam over a beam block situated on the beam axis. Electrostatic deflectors are employed to direct the ion beam through a 1 mm entrance aperture into the ultra-high-vacuum laser interaction and particle detection region.

Anions at $m/z = 35$ ($H_3O_2^-$) or $m/z = 38$ ($D_3O_2^-$) are intersected at a right angle by the third harmonic of a pulsed Ti : sapphire fundamental (258 nm, 1.2 ps FWHM) generated by a CPA2000 regenerative amplifier (Clark-MXR, Inc.) which is focused to a 0.5 mm diameter spot at the interaction region to give a fluence of approximately 5–10 mJ cm^{-2} $pulse^{-1}$. The $\boldsymbol{E}$ vector of the linearly polarized output was kept in the direction of the ion beam in all experiments. Photodetached electrons are detected by one of two time- and position-sensitive wedge-and-strip-anode electron detectors, which are placed opposite each other and perpendicular to the ion beam. Measurement of the electron recoil angle in this experiment is essential to allow correction for both the Doppler broadening due to the fast ion beam and the actual flight path in the large-solid-angle detector. With these corrections, the electron kinetic energy in the center-of-mass (CM) frame (eKE) is determined. The photoelectron spectrometer has an effective angular acceptance of ~20% of 4π sr. The resolution in eKE is ~5% $\Delta E/E$ at 1.3 eV.[25]

Residual ions remaining in the beam after the interaction region are electrostatically deflected out of the beam path to an ion detector, providing the TOF mass spectrum of the negative ions and a means of monitoring the ion beam intensity. The neutral photofragments can be measured with the photofragment translational spectrometer. Fragments recoil out of the beam over a 104 cm flight path and impinge on a time- and position-sensitive multi-particle detector made up of four quadrants, each of which is a separate crossed-delay-line detector, allowing determination of

the recoil velocities of two or more (up to eight) particles in coincidence. This information yields the photofragment mass ratio and CM translational energy (E_T).

This detector has been demonstrated to yield a photofragment translational energy resolution of $\sim$10% $\Delta E/E$ at 0.7 eV in recent studies of the three-body dissociation of O_6^-.[27] Since the electron and the photofragments are measured in coincidence, the correlated kinetic energy and angular distribution of the products are recorded in one experiment. During data analysis the events are sorted by the number and type of particle. All recorded events that produce one electron and two neutral photofragments are analyzed as correlated information for DPD, yielding the $N(E_T, \text{eKE})$ correlation spectrum. Statistics based on spectrometer efficiency and count rate of the experiment ensure that the photoelectron and photofragments from each event are correlated. Under the conditions of this experiment, a typical event rate of 0.13 per laser shot results in false coincidences of $\approx$2%.[28]

3. Results

3.A. Photoelectron–photofragment kinetic energy correlation: $H_3O_2^-$ and $D_3O_2^-$

The $N(E_T, \text{eKE})$ correlation spectrum at 258 nm (4.80 eV) is shown in Fig. 2 as a two dimensional histogram of the correlation between electron kinetic energy (eKE) along the y-axis and the photofragment translational energy release (E_T) along the x-axis. The one-dimensional spectra shown along each axis are obtained by integrating the correlation spectrum over the complementary variable, and represent the photoelectron kinetic energy and photofragment translational energy release spectra measurable in a conventional non-coincidence experiment. The photoelectron spectrum along the y-axis shows broad irregularly spaced features at eKE = 0.62, 1.15 and 1.49 eV and a shoulder at 0.95 eV which reproduces the published photoelectron spectrum by Arnold *et al.* at 266 nm.[9] The peak at 0.2 eV has a significant contribution from laser-produced photoelectron background. The photofragment translational energy release exhibits a broad peak centered

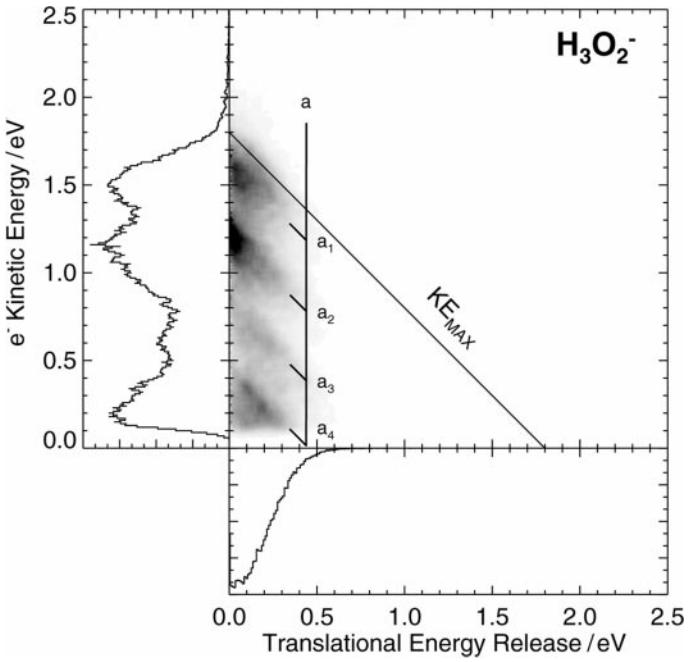

Fig. 2 Photoelectron–photofragment energy correlation spectrum ($N(E_T, \text{eKE})$) for $H_3O_2^- + h\nu \equiv H_2O + OH + e^-$ at 258 nm. The $N(E_T, \text{eKE})$ spectrum is represented as a two-dimensional gray-scale histogram. The histogram along the y-axis shows the photoelectron spectrum (eKE), and the x-axis shows the photofragment translational distribution (E_T). These are obtained by integrating the correlation spectrum over the complementary variable. The features and energetic limits shown are discussed in the text.

at $E_T = 0.05$ eV. The correlation spectrum, however, reveals considerably more information. The correlation of the broad peaks in the eKE and E_T spectra reveals a series of four diagonal ridges, (marked a in Fig. 2). The dominant features in the correlation spectrum are the diagonal ridges. All events that lie within a single diagonal ridge have a well-defined total kinetic energy, ($E_{TOT} = E_T + eKE$) because of energy conservation. Within a given ridge, however, there is a range of kinetic energy partitioning between the three products. Using the dissociation energy of $H_3O_2^-$ into H_2O and OH^- ($D_0 = 1.18$ eV) and the electron affinity of OH (EA = 1.828 eV)[19] the maximum translational energy:

$$KE_{MAX} = h\nu - D_0 - EA = 1.80 \text{ eV} \quad (2)$$

for the DPD process $H_3O_2^- + h\nu \rightarrow OH(^2\Pi, v = 0) + H_2O(X\,^1A_1, v = 0,0,0) + e^-$ at 258 nm is determined. This limit represents the dissociation asymptote and is marked as KE_{MAX} in Fig. 2. The ridges are separated by 0.42 eV, which is identified as a vibrational spacing in the H_2O or OH products (see section. 3.B.). The simplest explanation of these features is that they correspond to dissociative photodetachment (DPD) onto vibrationally adiabatic curves sensitive to the zero point energy effects of the potential. These adiabatic curves are located around the transition state for the neutral bimolecular reaction, and they correlate with the different vibrational states of the H_2O or OH products as discussed further below. Examination of the E_T distribution for each ridge individually shows that the width and shape of the spectrum depends on the product vibrational state, as shown in Fig. 3. The spectra are obtained by counting only events within a certain total kinetic energy range around the diagonal features. Starting at KE_{MAX} (1.80 eV) three equally spaced, 0.42 eV wide slices were used to generate Fig. 3. This energy width (0.42 eV) represents the spacings of the diagonal ridges. The first diagonal ridge (a_1) below KE_{MAX} peaks at $E_T = 0.05$ eV and extends to $E_T = 0.4$ eV, the second ridge (a_2) peaks near zero eV and extends to 0.4 eV. A remarkable shift in E_T is seen in the third ridge (a_3); it peaks at 0.12 eV and extends to 0.5 eV. The fourth ridge is suppressed by the detector cutoff function and the laser photoelectron background. This observation is consistent with the interpretation that these diagonal ridges correspond to different adiabatic curves in the transition state region corresponding to the product states, with different curvatures (see Discussion). In other words, in this experiment we directly probe the

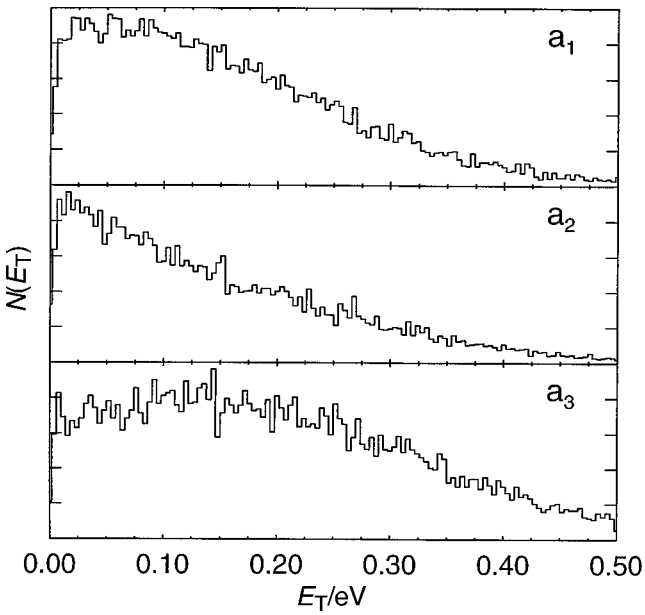

Fig. 3 Kinetic energy release ($N(E_T)$) for $H_3O_2^- + h\nu \equiv H_2O + OH + e^-$ at 258 nm for different diagonal ridges individually, as marked in Fig. 2.

vibrational thresholds for the bimolecular reaction by measuring the photoelectrons and photofragments in coincidence.

The correlation spectrum for the deuterated compound ($D_3O_2^-$) is shown in Fig. 4. As noted by Arnold *et al.*,[9] the peak position and intensities in the photoelectron spectrum change upon deuteration. This indicates that the observed peaks are related to hydrogen motion of the dissociative neutral complex formed by photodetachment. Arnold *et al.*[9] discussed this observation in terms of a one-dimensional Franck–Condon analysis and assigned these features to the O ← H → O antisymmetric stretch motion of the transfer hydrogen in the unstable neutral [HOHOH] complex. The fragment translational energy spectrum shifts to higher kinetic energy in the deuterated compound and peaks at 0.12 eV. This may arise from the lower zero point energy in the deuterated anion leading to contraction of the wavefunction, giving better Franck–Condon overlap with a repulsive region on the potential energy surface near the transition state upon photodetachment. The correlation spectrum shows five diagonal ridges spaced by 0.33 eV (see section 3.B.). Due to the change in the zero point energy (ZPE) in the anion complex and in the products upon deuteration (ΔZPE), KE_{MAX} shifts to higher energy. The difference in the zero point energies upon deuteration (ΔΔZPE) can be estimated to be ΔΔZPE = 0.17 eV.[29] This yields an estimate for KE_{MAX} = 1.97 eV, in good agreement with our experimental value of KE_{MAX} = 1.95 eV. In comparison to the nondeuterated case, examination of the E_T distribution within a given ridge shows a similar, but less expressed behavior. E_T for the first diagonal ridge below KE_{MAX} peaks at 0.12 eV and extends to 0.5 eV, the second ridge peaks at 0.10 eV and extends to 0.55 eV, and the third ridge peaks at 0.13 eV and extends to 0.55 eV. In the deuterated case, the biggest shift in E_T is seen in the fourth ridge; it peaks at 0.15 eV and extends to 0.56 eV. The fifth ridge is suppressed by the detector cutoff function. The observation of five ridges in the deuterated case compared to four in the nondeuterated case shows that zero point effects along the hydrogen transfer coordinate on the neutral surface play a key role in the reaction dynamics of the bimolecular reaction.

3.B. Total kinetic energy release spectra of $H_3O_2^-$ and $D_3O_2^-$ at 258 nm

Another informative way to view the $N(E_T, eKE)$ correlation spectra is by direct examination of the total translational energy spectra generated by summing the photoelectron kinetic energy and

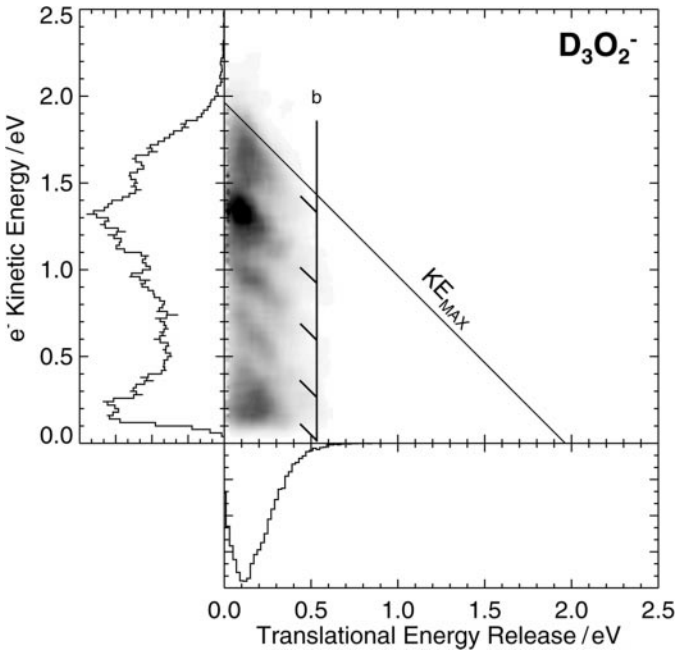

Fig. 4 Photoelectron–photofragment energy correlation spectrum ($N(E_T, eKE)$) for $D_3O_2^- + h\nu \equiv D_2O + OD + e^-$ at 258 nm. $N(E_T, eKE)$ is represented as a two-dimensional gray-scale histogram. See the text and caption for Fig. 2 for discussion of the features and energetic limits shown.

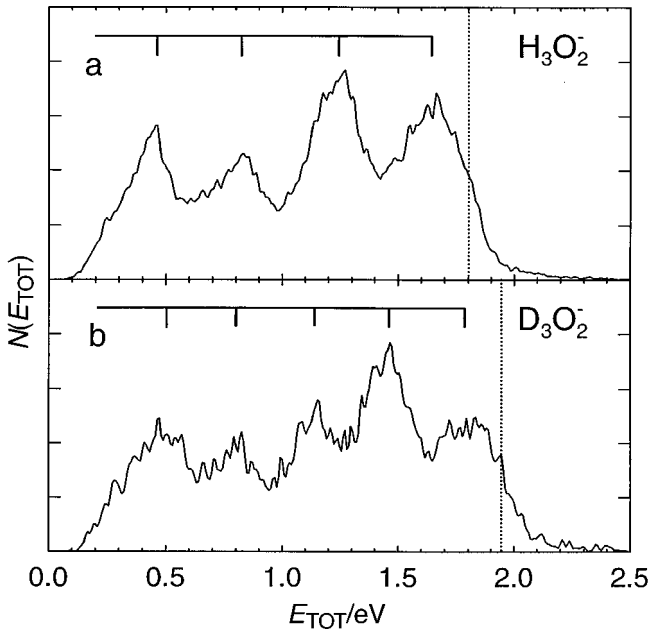

Fig. 5 Vibrationally resolved product translational energy ($N(E_{TOT})$) spectra for the DPD of $H_3O_2^-$ and $D_3O_2^-$ at 258 nm as labeled. The dashed lines represent the dissociation asymptotes as marked as KE_{MAX} in Figs. 2 and 4.

the translational energy release for each event: $E_{TOT} = eKE + E_T$. The $N(E_{TOT})$ spectra for $H_3O_2^-$ and $D_3O_2^-$ are shown in Fig. 5. Now the diagonal features in the $N(E_T, eKE)$ spectra appear as a resolved spectrum of the correlated product vibrational distribution. Examination of the offset of the vibrational peaks from the internal energy origin ($KE_{MAX} = 1.80$ eV) for $H_3O_2^-$ in this spectrum gives a sum for the rotational energy of OH and H_2O and bending excitation in H_2O of 150 ± 30 meV. There is no experimental evidence for bending excitation, however *ab initio* calculations suggest some excitation in the bending mode, because removal of one electron leads

Table 1 Peak positions and widths for the total kinetic energy spectra of $H_3O_2^-$ and $D_3O_2^-$

Peak	E_{TOT}/eV	Internal energy/eV[a]	Peak width/eV[b]
$H_3O_2^-$			
a_1	1.64	0.0	0.16
a_2	1.23	0.41	0.16
a_3	0.81	0.83	0.20
a_4	0.44	1.20	—
$D_2O_2^-$			
b_1	1.79	0.0	0.19
b_2	1.45	0.34	0.15
b_3	1.14	0.65	0.16
b_4	0.79	1.00	0.17
b_5	0.48	1.31	—

[a] Internal in the $OH + H_2O$, or $OD + D_2O$ product respectively. [b] Full width at half maximum (FWHM) as determined by fit to a Gaussian shaped peak, due to the electron detector cutoff function and laser background no width could be measured for the peaks at low photoelectron energy.

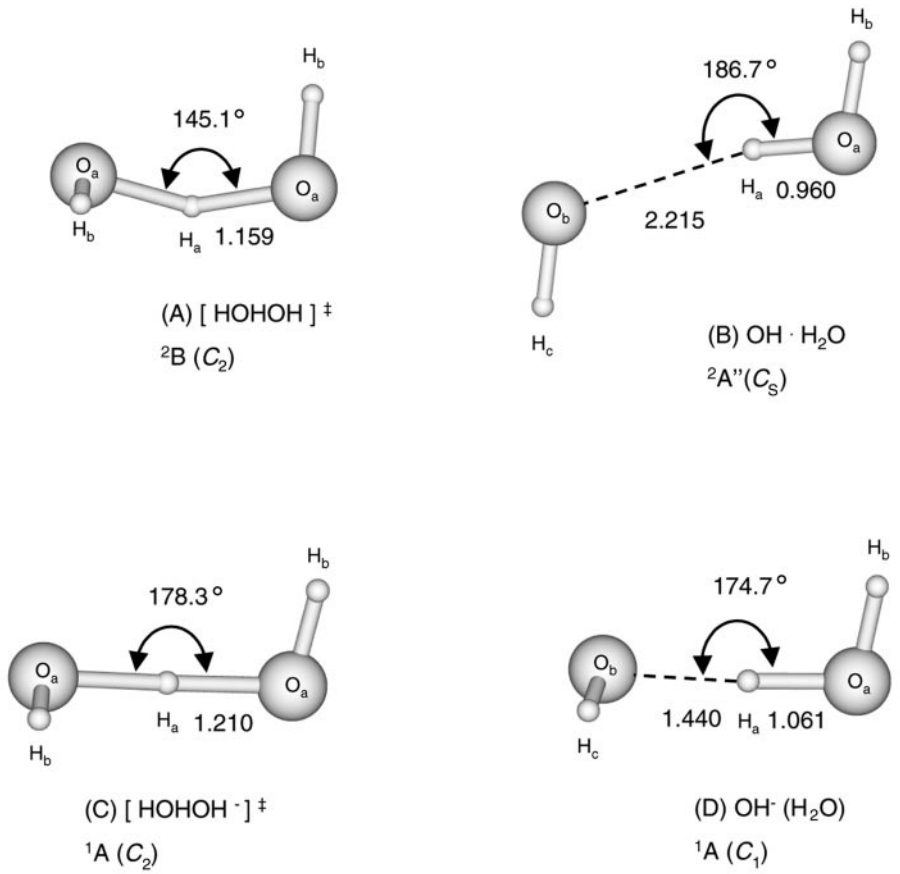

Fig. 6 Calculated (UQCISD 6-311++G(d,p)) stationary points of the neutral $H_2O + OH$ reaction: (A) transition state [HOHOH], (B) van der Waals complex and the $H_3O_2^-$ anion: (C) [$HOHOH^-$] transition state and (D) $OH^-(H_2O)$ minimum structure. Selected parameters are in Å and in degrees.

to a structure slightly more bent than in the anion (see sections 3.C. and 4.). The remarkably narrow rotational distribution of the H_2O and OH products implies $H_3O_2^-$ undergoes DPD from a well-defined symmetric structure and thus low exit channel impact parameter. Table 1 lists the observed peak positions and widths for both systems. Since the observed peak spacings are quite regular in $H_3O_2^-$ ($\sim$0.42 eV = 3388 cm^{-1}), it is useful to compare them to the observed vibrational frequencies of the possible products OH ($\omega_e = 3737$ cm^{-1})[30] and H_2O ($\nu_1 = 3657$, $\nu_2 = 1595$, $\nu_3 = 3756$ cm^{-1}).[31] The observed spacings are in reasonable agreement with the stretching frequencies of the OH and the H_2O molecule. Due to the lower zero point energy of the deuterated products D_2O and OD the $N(E_{TOT})$ spectrum of $D_3O_2^-$ shifts to higher energies (see also section 3.A.) and the spacing between the first four peaks is reduced to 0.33 eV (2662 cm^{-1}), close to the stretching frequencies in OD ($\omega_e = 2720$ cm^{-1})[30] and D_2O ($\nu_1 = 2671$, $\nu_3 = 2788$ cm^{-1}).[32] Compared to the photoelectron spectrum, the total kinetic energy spectrum shows more structure and a nicely resolved progression in the nondeuterated and deuterated case. This behavior is expected for systems undergoing DPD with constrained product energy distributions, as previously observed in our studies of DPD of O_4^-.[33]

3.C. Electronic structure calculations

To aid in the analysis of the data presented above, *ab initio* calculations were performed using the GAUSSIAN 94 program package[34] for the anion and neutral complexes involved in these experi-

Table 2 Optimized geometries (bond lengths, Å; angles, °), vibrational frequencies (cm^{-1}), total energies (E_h), zero point energies (ZPE) (E_h per particle) of the stationary points along the reaction path for the $OH^- + H_2O$ hydrogen atom transfer in the anion

Species	Parameter	This work (UQCISD(fc)6-311++G(d,p))	Ref. 12 (MP2 aug-cc-pVDZ)
OH^-	O–H	0.9645	0.973
	Frequency	3780	3767
	ZPE	0.008 610	0.008 574
	Total energy	−75.640 303	−75.639 281
H_2O	O–H	0.959	0.957
	H–O–H	103.6	102.5
	Frequencies	1654, 3889, 3991	1668, 3909, 4017
	ZPE	0.021 722	0.021 855
	Total energy	−76.281 753	−76.263 97
$HO^-(H_2O)$ (C_1)	O_a–H_a	1.061	1.089
	O_b–H_a	1.440	1.426
	O_a–H_b	0.958	0.959
	O_b–H_c	0.961	0.961
	O_a–H_a–O_b	174.7	177.9
	H_a–O_a–H_b	108.1	105.0
	H_a–O_b–H_c	100.6	102.0
	O_a–H_a–O_b–H_c	336.9	334.0
	O_b–H_a–O_a–H_b	92.8	101.3
	Frequencies	198, 291, 429, 592, 1307, 1736, 2046, 3854, 3922	207, 328, 453, 570, 1321, 1608, 1729, 3814, 3864
	ZPE	0.032 750	0.031 650
	Total energy	−151.965 803	−151.945 438
			Ref. 16 (MP2 6-31+G(d,p))
$[HOHOH^-]‡$ (C_2)	O_a–H_a	1.210	1.221
	O_a–H_b	0.959	0.966
	O_a–H_a–O_a	178.0	—
	H_a–O_a–H_b	102.7	—
	Dihedral	55.2	—
	Frequencies	*i* 761, 210.2468, 560, 580, 665, 1523, 1682, 3887, 3888	*i* 1028, —
	ZPE	0.029 606	0.028 367 2
	Total energy	−151.965 104	−151.959 180

ments. The main goal was to calculate the electronic structures of the stationary points in the neutral and the anion consistently and to find a method that is accurate enough for calculation of the potential energy surfaces for both the anion and the neutral in the future (see section 5.). High level *ab initio* calculations are presumed to be essential due to the open shell character of the neutral. Since the UMP2 method failed to predict the symmetric nature of the [HOHOH]‡ transition state of the neutral bimolecular reaction,[21–23] the structures of the stationary points on the neutral surface have been optimized at the unrestricted quadratic configuration interaction with singles and doubles excitation (UQCISD) level of theory. While the oxygen 1s electrons were frozen at the UHF level (frozen core (fc)), all other electrons were included in the calculation of the correlation energy. To maintain consistency, the stationary points on the anion surface have been calculated at the same level of theory. In both cases the standard 6-311++G(d,p) basis set was used. The nature of each stationary point was established by a harmonic force field frequency calculation using numerical energy second derivatives. In order to achieve high accuracy in determination of the energetics of the system, we performed single point UQCISD(T) calculations, including triples excitation non-iteratively, in the frozen core approximation employing the 6-311++G(3df,2p) basis set at the geometries optimized at the UQCISD level for the stationary points (UQCISD(T) 6-311++G(3df,2p)//UQCISD 6-311++G(d,p)).

Previous *ab initio* studies on the $H_3O_2^-$ anion have been carried out.[9–14] The optimized structures for the anion and the transition state for hydrogen transfer in the anion found in the presented work are shown in Fig. 6. The internal coordinates and the harmonic frequencies are listed in

Table 3 Total energies (E_h), electron affinity (EA in eV), barrier height (E_0 in eV) and association energies (E_{as} in eV), and dissociation energy of the anion (D_0 in eV) (zero point energies, see Tables 2 and 4)

Structure	UQCISD(T)(fc) 6-311 + + G(3df,2p)	EA/eV	D_0/eV	E_0/eV	E_{as}/eV
OH^-	−75.696 648				
H_2O	−76.332 062				
$OH^-\cdots H_2O$	−152.028 624				
Supermolecule					
$OH^-(H_2O)$ (C_1)	−152.073 237		1.15		
$[HOHOH^-]‡$ (C_2)	−152.072 734				
OH	−75.637 046	1.62			
$OH\cdots H_2O$	−151.969 107				
Supermolecule					
$OH^{\cdot}(H_2O)$ (C_s)	−151.973 484				0.10
van der Waals complex					
[HOHOH]‡ (C_2)	−151.953 275			0.42	
Expt. (reference)		1.83[a]	1.18[d]		
Calc. (reference)		1.59[b]		0.44[e]	0.15[f]
		1.87[c]			

[a] Ref. 19. [b] Ref. 36. [c] Ref. 35. [d] Ref. 18. [e] Ref. 23. [f] Ref. 20.

Table 2. In agreement with the most recent study,[12] we find that the water molecule binds to the oxygen atom of the hydroxide ion *via* an almost linear bond. We calculated a dissociation energy of 1.15 eV for this hydrogen bond (Table 3), giving very good agreement with the experimental value of 1.18 eV.[18] The fact that this hydrogen bond is very strong results in a large distortion of the water molecule in this complex. The hydrogen bonded $R(O_a–H_a)$ bond distance is 1.061 Å,

Table 4 Optimized geometries (bond lengths, Å; angles, °), vibrational frequencies (cm^{-1}), total energies (E_h), zero point energies (E_h per particle) of the stationary points along the reaction path for the OH + H_2O hydrogen atom transfer in the neutral

Species	Parameter	This work (UQCISD(fc)6-311 + + G(d,p))	Ref. 23 (UMP2/6-311 + + G(d,p))
OH	O–H	0.971	0.966
	Frequency	3776	3858
	ZPE	0.008 603	0.008 791
	Total energy	−75.593 469	−75.572 900
$HO^{\cdot}(H_2O)$ (C_s)	$O_a–H_a$	0.960	0.962
	$O_b–H_a$	2.216	2.098
	$O_a–H_b$	0.958	0.958
	$O_b–H_c$	0.970	0.969
	$O_a–H_a–O_b$	186.7	199.3
	$H_a–O_a–H_b$	103.5	103.9
	$H_a–O_b–H_c$	158.6	109.2
	Frequencies	76, 101, 129, 296, 341, 1556, 3796, 3882, 3950	74, 113, 145, 307, 359, 1742, 4048, 4128, 4254 (UHF)
	ZPE	0.031 407	0.034 581 (UHF)
	Total energy	−151.880 914	—
[HOHOH]‡ (C_2)	$O_a–H_a$	1.159	1.139
	$O_a–H_b$	0.967	0.964
	$O_a–H_a–O_b$	145.1	140.1
	$H_a–O_a–H_b$	102.2	102.0
	Dihedral	62.4	59.1
	Frequencies	*i* 2842, 385, 452, 580, 934, 1406, 1521, 3839, 3845	386, 504, 619, 970, 1352, 1734, 1891, 3882, 3885
	ZPE	0.029 529	0.034 680
	Total energy	−151.855 041	−151.819 770

while the "free" $R(O_a–H_b)$ length remains nearly unchanged with respect to water, and the $(H_a–O_a–H_b)$ angle is 100.62°. The nuclear arrangement at the equilibrium geometry readily allows for isomerization *via* transfer of H_a between the two oxygen atoms O_a and O_b (see Fig. 6). The electronic energy barrier is very small (0.014 eV at the UQCISD(T) 6-311++G(3df,2p)//UQCISD 6-311++G(d,p) level of theory). Inclusion of the zero point energy correction stabilizes the symmetric transition state more than the asymmetric minimum, resulting in a barrierless motion of the hydrogen bonded proton between the two oxygen atoms. An extensive quantum dynamics study by Parrinello *et al.*[17] found an effective single well potential with a centrosymmetric distribution of the shared proton.

For the discussion of both the anion and the neutral potential surfaces, a proper description of the electron affinity of the hydroxyl radical is important. The calculated value of 1.62 eV (see Table 3) is in reasonable agreement with experiment (1.828 eV)[19] compared to other *ab initio* studies.[35,36]

In Table 4 the geometries for the reactants, the van der Waals complex and the transition state of the hydrogen exchange reaction (1) in the neutral are listed in comparison with the most detailed study by Balint-Kurti and co-workers.[23] In agreement with their calculated potential barrier height $E_0 = 0.44$ eV for the symmetric hydrogen atom exchange reaction we find a value of $E_0 = 0.42$ eV at the UQCISD(T) 6-311++G(3df,2p)//UQCISD 6-311++G(d,p) level of theory (see Table 3). The UQCISD 6-311++G(d,p) approach optimized the transition state in the C_2-symmetry, expected for this reaction.[21–23] In conclusion, our theoretical approach is capable of calculating the electronic structures and energetics of the $H_3O_2^-/OH + H_2O$ system in good agreement with experiment and recent *ab initio* studies. This should provide a practical method for carrying out a more extensive calculation of the relevant potential energy surfaces.

4. Discussion

The data presented here provide detailed experimental insights into the dynamics of the DPD of $H_3O_2^-$. Fig. 7 summarizes the data obtained in these experiments. The $H_3O_2^-$ anion is placed at -3.01 eV (EA(OH) + $D_0(H_3O_2^- \rightarrow OH^- + H_2O)$) relative to the $OH + H_2O + e^-$ dissociation asymptote. The photon energy for 258 nm photodetachment is plotted relative to this $H_3O_2^-$ origin. The E_T spectrum at 258 nm provides an average measure of the photofragment repulsion and is plotted with $E_T = 0$ at the $OH + H_2O + e^-$ dissociation asymptote. The 258 nm photoelectron spectrum is plotted as the photoelectron binding energy $E_{bind} = E_{h\nu} - eKE$. Finally, the total translational energy release spectrum at 258 nm (section 3.B.) is shown plotted with $E_{TOT} = 0$ at the 258 nm photon energy.

Since the photoelectron spectrum is determined by the Franck–Condon overlap between the bound anion ground state wavefunction and the scattering wavefunction on the neutral surface it is useful to compare the calculated geometries (Fig. 6) for the anions (Table 2) and the neutral (Table 4) transition state. The very flat effective single well anion potential[9,17] results in an extended hydrogen atom motion and a large Franck–Condon region for the photodetachment process. A comparison of the C_2-symmetric anion geometry, where the wavefunction has the largest amplitude[17] (Fig. 6C) and the calculated C_2-symmetric transition state geometry (Fig. 6A) predicts a reasonable overlap between the anion and the neutral geometries. The bond distances between the transfer hydrogen atom and the oxygen atoms is contracted from 1.210 to 1.159 Å and the OHO bond angle is also slightly contracted, with the anion being more linear (178.3°) than in the transition state (145.1°). The other structural parameters do not significantly change upon removal of one electron. Thus the center of the Franck–Condon region will be slightly away from the saddle point toward the entrance and exit channels. Significant Franck–Condon overlap with the van der Waals complex (Fig. 6B) is not expected, given the geometry of the anion.

The one-dimensional Franck–Condon analysis carried out by Arnold *et al.*[9] using *ab initio* potentials for the anion and the neutral was able to reproduce both the $H_3O_2^-$ and $D_3O_2^-$ photoelectron spectra reasonably well. Due to symmetry considerations[31] only transitions to even states of the neutral ($v' = 2m$, where v' is the vibrational quanta of the antisymmetric stretch of the transfer hydrogen atom in the neutral complex [HOHOH] after photodetachment and $m = 0,1,2,3 \cdots$) have nonzero intensity. The simulation of Arnold *et al.* represents photodetachment transitions to the $v' = 0$, $v' = 2$, and $v' = 4$ vibrational states supported by the neutral potential energy

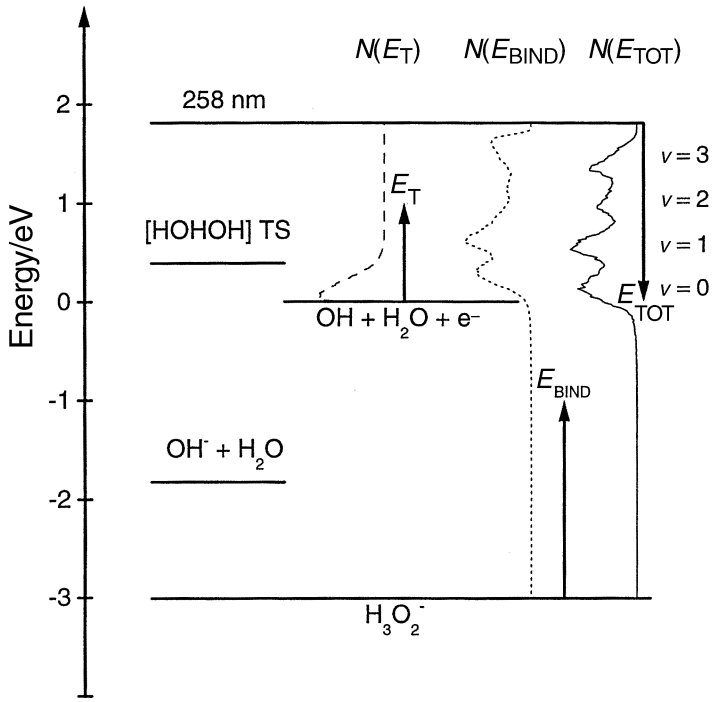

Fig. 7 Energetics of the dissociative photodetachment of $H_3O_2^-$. The dissociation asymptote, $OH + H_2O + e^-$, is shown as the zero of energy. The vertical short-dashed spectrum shows the photoelectron spectrum at 258 nm as the electron-binding energy ($N(E_{Bind})$) relative to $H_3O_2^-$. The vertical long-dashed spectrum shows $N(E_T)$ at 258 nm, with $E_T = 0$ at $OH + H_2O + e^-$. Finally the vertical solid line spectrum shows the 258 nm total translational energy spectrum $N(E_{TOT})$, plotted with $E_{TOT} = 0$ at the 258 photon energy. The origin and direction of increasing energy for each spectrum is indicated by the arrows. Product H_2O antisymmetric vibrational states are labeled by $v = 0, 1, 2, 3$.

surface.[9] Solving the time independent Schrödinger equation in one dimension to determine the antisymmetric stretch energy levels and wavefunctions for a similar symmetric hydrogen atom transfer reaction ($Br + HBr \rightarrow BrH + Br$) Neumark *et al.*[2b] calculated the vibrationally adiabatic curves corresponding to this antisymmetric mode. They showed that at an asymptotic separation of the products, the $v' = 2m$ and $v' = 2m + 1$ antisymmetric stretch states of the complex become degenerate and correlate to the $v = m$ vibrational state of the diatomic product. In the diatom–triatom reaction under consideration here, it is expected that this asymptotic product state will be the antisymmetric stretch of the H_2O product. The *ab initio* calculations presented above also show that the OH bond lengths of the two hydrogen atoms not involved in the hydrogen atom exchange change only slightly, and can be seen as "spectator" bonds. Our results on the total kinetic energy release $N(E_{TOT})$ in combination with the calculated electronic structures suggests that the first three peaks are due to H_2O antisymmetric stretching vibrations (0,0,0), (0,0,1), (0,0,2) in the H_2O product correlating adiabatically to the $v' = 2m$ states at the transition state of the bimolecular reaction.

The observation of the diagonal structure in the photoelectron–photofragment $N(E_T, eKE)$ spectra illustrates the value of coincidence measurements for the study of DPD processes and also provide firm evidence that the DPD of $H_3O_2^-$ is a direct process probing the transition state region of the neutral bimolecular reaction. The DPD of $H_3O_2^-$ is an example of photoabsorption into two continua—the photoelectron and the photofragment dissociation continua. The diagonal ridges observed in the $N(E_T, eKE)$ correlation spectrum result from projection of the wavefunction describing bound $H_3O_2^-$ onto the repulsive nuclear potential describing $OH + H_2O + e^-$ in a bound-to-free Franck–Condon absorption. The measurement of E_T in this case provides information that is complementary to the eKE measurement, since E_T is a direct measure of the repul-

sive energy relative to the dissociation asymptote. The length of the projections of these ridges onto the E_T and eKE axes is a function of both the average distance along the bound coordinate in $H_3O_2^-$ and the slope of the nuclear potential along the reaction coordinate that governs the dissociation to H_2O and OH. The steeper the slope of the repulsive potential to each product state, the longer the ridge in the $N(E_T, \mathrm{eKE})$ correlation spectrum. The results presented in section 3.A. show different lengths for the projection of E_T in the different vibrational thresholds observed in both the nondeuterated and the deuterated case. These results indicate that the different vibrational states formed by photodetachment decay on adiabatic curves with varying slopes in the Franck–Condon region. As mentioned in section 3.A. we find that the kinetic energy release is peaked near zero in the second ridge in both the nondeuterated and deuterated spectrum. This is a consequence of a variation in intensity along the corresponding diagonal ridge. This second ridge corresponds to the $v' = 2$ state in the photoelectron spectrum and $v = 1$ in the antisymmetric stretch of the H_2O product. This vibrationally excited state is energetically located at the top of the calculated barrier to the reaction. There are two plausible explanations for this feature. The first one is that there is Franck–Condon overlap with the van der Waals entrance channel complex on one of the vibrationally excited adiabatic curves. In the resulting dissociation, the partitioning of energy would have to be such that the kinetic energy release (E_T) placed the feature on one of the diagonal ridges. A second, more interesting possibility is that this is a signature of photodetachment to a quasi-bound state of the $OH–H_2O$ collision complex. Variations in intensity along the diagonal ridge in the correlation spectrum as seen in both systems under study here, can be thought of as a measure of the varying bound–free Franck–Condon overlap for photodetachment from the anion to the repulsive neutral surface. If a quasi-bound complex is accessed at some part along the adiabatic curve, the higher oscillator strength might lead to the observed distribution.

5. Conclusion

This paper reports a high resolution photoelectron–photofragment coincidence study of $H_3O_2^-$ and $D_3O_2^-$. These measurements provide insights into the half-collision dynamics of the neutral symmetric hydrogen exchange reaction. In a qualitative analysis using *ab initio* electronic structure calculations on the QCISD level of theory we assigned the observed product state distribution to the antisymmetric stretch of the water product.

Further theoretical work is required to extract more information from the presented results. We are currently working on calculating a reduced, two dimensional *ab initio* potential energy surface for the anion and the neutral in the oxygen–hydrogen bond distances of the transfer hydrogen atom. Using these surfaces a quantum dynamics calculation will be performed to simulate the photoelectron spectra, the translational energy release and the product state distribution. A crucial test for this treatment will be if these simulations can reproduce the variation of the kinetic energy release observed in the different product vibrational states and simulate the possible signature of the quasi-bound states.

Acknowledgements

This work was supported by the Department of Energy (DOE) under Grant No. DE-FG03-98ER14879. H.-J.D. is supported by a "Forschungsstipendium der Deutschen Forschungsgemeinschaft" and the DOE. A.K.L. and T.G.C. are supported under AFOSR grants AASERT F49620-97-1-0387 and F49620-96-1-0220. R.E.C. is a Camille Dreyfus Teacher–Scholar, and an Alfred Sloan Research Fellow and a Packard Fellow in Science and Engineering. We also want to acknowledge Prof. P. R. Taylor and T. Ruden for fruitful discussion concerning *ab initio* calculations.

References

1 R. E. Continetti, *Int. Rev. Phys. Chem.*, 1998, **17**, 227.
2 (*a*) D. M. Neumark, *Acc. Chem. Res.*, 1993, **26**, 33; (*b*) R. B. Metz, S. E. Bradforth and D. M. Neumark, *Adv. Chem. Phys.*, 1992, **81**, 1.

3 P. G. Wenthold and W. C. Lineberger, *Acc. Chem. Res.*, 1999, **32**, 597.
4 J. M. Farrar, in *Cluster Ions*, ed. T. Bear, C. Y. Ng and I. Powis, Wiley, New York, 1993, p. 243.
5 K. M. Ervin and W. C. Linberger, in *Advances in Gas Phase Ion Chemistry*, ed. N. G. Adams and L. M. Babcock, JAI Press, Greenwich, CT, 1992, vol. 1.
6 R. Atkinson, *Chem. Rev.*, 1986, **86**, 69.
7 M. K. Dubey, R. Mohrschladt, N. M. Donahue and J. G. Anderson, *J. Phys. Chem. A*, 1997, **101**, 1494.
8 S. Golub and B. Steiner, *J. Chem. Phys.*, 1968, **49**, 5191.
9 D. W. Arnold, C. Xu and D. M. Neumark, *J. Chem. Phys.*, 1995, **102**, 6088.
10 C. M. Rohlfing, L. C. Allen, C. M. Cook and H. B. Schlegel, *J. Chem. Phys.*, 1983, **78**, 2498.
11 J. E. Bene, *J. Phys. Chem.*, 1988, **92**, 2874.
12 S. S. Xantheas, *J. Am. Chem. Soc.*, 1995, **117**, 10373.
13 C. P. Valle and J. J. Novoa, *Chem. Phys. Lett.*, 1997, **269**, 401.
14 L. R. Corrales, *J. Chem. Phys.*, 1999, **110**, 9071.
15 M. M. Szczęśniak and S. Schreiner, *J. Chem. Phys.*, 1982, **77**, 4586.
16 S. Gronert, *J. Am. Chem. Soc.*, 1993, **115**, 10258.
17 M. E. Tuckerman, D. Marx, M. L. Klein and M. Parrinello, *Science*, 1997, **275**, 817.
18 Represents the average of the two values (26.8 (*a*) and 27.6 kcal mol − 1 (*b*)) in the following references: (*a*) M. Meot-Ner (Mautner) and L. W. Sieck, *J. Phys. Chem.*, 1986, **90**, 6687; G. J. C. Paul and P. Kebarle, *J. Phys. Chem.*, 1990, **94**, 5184.
19 P. A. Schulz, R. D. Mead, P. L. Jones and W. C. Lineberger, *J. Chem. Phys.*, 1982, **77**, 1153.
20 (*a*) K. S. Kim, H. S. Kim, J. H. Jang, H. Soon, B.-J. Mhin, Y. Xie and H. F. Schaefer, *J. Chem. Phys.*, 1991, **94**, 2057; (*b*) Y. Xie and H. F. Schaefer, *J. Chem. Phys.*, 1993, **98**, 8829.
21 A. A. Nanayakkara, G. G. Balint-Kurti and I. H. Williams, *J. Phys. Chem.*, 1992, **96**, 3662.
22 H. Basch and S. Hoz, *J. Phys. Chem. A*, 1997, **101**, 4416.
23 M. R. Hand, C. F. Rodriquez, I. H. Williams and G. G. Balint-Kurti, *J. Phys. Chem. A*, 1998, **102**, 5958.
24 K. A. Hanold, C. R. Sherwood, M. C. Garner and R. E. Continetti, *Rev. Sci. Instrum.*, 1995, **66**, 5507.
25 K. A. Hanold, A. K. Luong, T. G. Clements and R. E. Continetti, *Rev. Sci. Instrum.*, 1999, **70**, 2268.
26 M. A. Johnson and W. C. Lineberger, in *Techniques in Chemistry*, ed. J. M. Farrar and W. H. Saunders, 1988, vol. 20, p. 591.
27 K. A. Hanold, A. K. Luong and R. E. Continetti, *J. Chem. Phys.*, 1998, **21**, 9215.
28 R. E. Continetti, *Photoionization and Photodetachment*, in Adv. Ser. Phys. Chem., ed. C. Y. Ng, World Scientific, Singapore, in press.
29 Difference in zero point energies $\Delta\Delta ZPE = \Delta ZPE(H_2O - D_2O) + \Delta ZPE(OH - OD) - \Delta ZPE(H_3O_2^- - D_3O_2^-)$; where $\Delta ZPE(H_2O - D_2O) = 0.154$ eV, ref. 30; $\Delta ZPE(OH - OD) = 0.062$ eV, ref. 30; $\Delta ZPE(H_3O_2^- - D_3O_2^-) \approx \Delta_{f,0\,K}H^0(H_3O_2^- - D_3O_2^-) = 0.042$ eV, where $\Delta_{f,0}H^0(H_3O_2^-) = \Delta_{f,298}H^0(H_3O_2^-)$ − thermal correction (MP2 6-311++G(d,p)), where $\Delta_{f,298}H^0(H_3O_2^-) = -117.4$ kcal mol^{-1}, ref. 18(*b*) and $\Delta_{f,0}H^0(D_3O_2^-) = \Delta_{f,298}H^0(D_3O_2^-)$ − thermal correction (MP2) 6-311++G(d,p)), where $\Delta_{f,298}H^0(D_3O_2^-) = -118.2$ kcal mol^{-1}, ref. 18(*a*).
30 G. Herzberg, *Molecular Spectra and Molecular Structure I. Spectra of Diatomic Molecules*, Krieger, Malabar, 1965.
31 G. Herzberg, *Molecular Spectra and Molecular Structure III. Electronic Spectra and Electronic Structure of Polyatomic Molecules*, Krieger, Malabar, 1965.
32 T. Shimanouchi, *Tables of Molecular Vibrational Frequencies Consolidated Volume 1*, National Bureau of Standards, 1972, p. 1.
33 K. A. Hanold and R. E. Continetti, *Chem. Phys.*, 1998, **239**, 493.
34 Gaussian 94, Revision C.3, M. J. Frisch, G. W. Trucks, H. B. Schlegel, P. M. W. Gill, B. G. Johnson, M. A. Robb, J. R. Cheeseman, T. Keith, G. A. Petersson, J. A. Montogomery, K. Raghavachari, M. A. Al-Laham, V. G. Zakrzewski, J. V. Ortiz, J. B. Foresman, J. Cioslowski, B. B. Stefanov, A. Nanayakkara, M. Challacombe, C. Y. Peng, P. Y. Ayala, W. Chen, M. W. Wong, J. L. Andres, E. S. Replogle, R. Gomperts, R. L. Martin, D. J. Fox, J. S. Binkley, D. J. Defrees, J. Baker, J. P. Stewart, M. Head-Gordon, C. Gonzalez and J. A. Pople, Gaussian Inc., Pittsburgh, PA, 1995.
35 J. Hrušák, H. Friedrichs, H. Schwarz, H. Razafinjanahary and H. Chermette, *J. Chem. Phys.*, 1996, **100**, 100.
36 H.-J. Werner, P. Rosmus and E.-A. Reinsch, *J. Chem. Phys.*, 1983, **79**, 905.